Supporting Information

Revealing the key factors affecting the anode performance of metal-ion batteries: a case study of boron carbide monolayers

Shicong Ding[1], Xu Yan[1], Javed Rehman[2,*], Sheng Wang[1], Yong Liu[1], and Guochun Yang[1,3*]

[1]*State Key Laboratory of Metastable Materials Science & Technology and Key Laboratory for Microstructural Material Physics of Hebei Province, School of Science, Yanshan University, Qinhuangdao 066004, China*
[2]*State Key Laboratory of Metastable Materials Science and Technology, School of Materials Science and Engineering, Yanshan University, Qinhuangdao 066004, China*
[3]*Centre for Advanced Optoelectronic Functional Materials Research and Key Laboratory for UV Light-Emitting Materials and Technology of Northeast Normal University, Changchun 130024, China*
Corresponding Authors: javedktk15@ysu.edu.cn and yanggc468@nenu.edu.cn

Index **Page**

Computational Details

The particle swarm optimization (PSO) method, integrated within the evolutionary algorithm and implemented in the Crystal structure AnaLYsis by Particle Swarm Optimization (CALYPSO) code,[1, 2] was employed to identify the lowest-energy structures of B_yC_x (x = 3–12, y = 1; x = 3, 5, 7, 9, 11, y = 2). Specifically, the number of layers was set to 1, the layer thickness was set to 0.2 Å, and a vacuum layer of 20 Å along the c-axis was introduced to prevent interlayer interactions, which were consistent with previously reported values.[3, 4] Initially, random structures with specific symmetry were generated, where atomic coordinates were produced through crystallographic symmetry operations. Subsequent local optimizations were performed using the VASP code,[5, 6] under a version with a fixed c-axis, employing the conjugate gradients method and terminating when the total energy changes fell below 1×10^{-5} eV per cell. Following the processing of the initial generation structures, 60% of those with lower enthalpies were selected to generate the subsequent generation structures via PSO. Additionally, 40% of the structures in the new generation were randomly created. Structural searches were carried out for 1–4 formula units, with a maximum of 30 atoms. Each generation consisted of 40 structures, and the calculations were iterated over at least 20 generations.

The scanning potential energy surface was constructed by calculating the energy of a single K atom at various positions above the B–C monolayer. A Python script[7] was employed to automatically generate these positions, using the relaxed CONTCAR file of the optimal adsorption site within a 2 × 2 supercell as the input to determine the ideal adsorption height. For the BC_6 and BC_8 monolayers, 12 positions were generated in both the x and y directions, resulting in a total of 144 positions. Additionally, for the BC_{11} monolayer, 12 positions were generated in the x direction and 8 in the y direction, totaling 96 positions. Relaxation for each position was performed using VASP code.[5, 6] Given that most sites are not conducive to K atom adsorption, the K atom was constrained to move only vertically to achieve adsorption equilibrium. Upon completing the calculations, the Python script extracted the data and plotted the potential energy surface by calculating the energy differences between each site and the optimal adsorption site.

Supplementary Figures

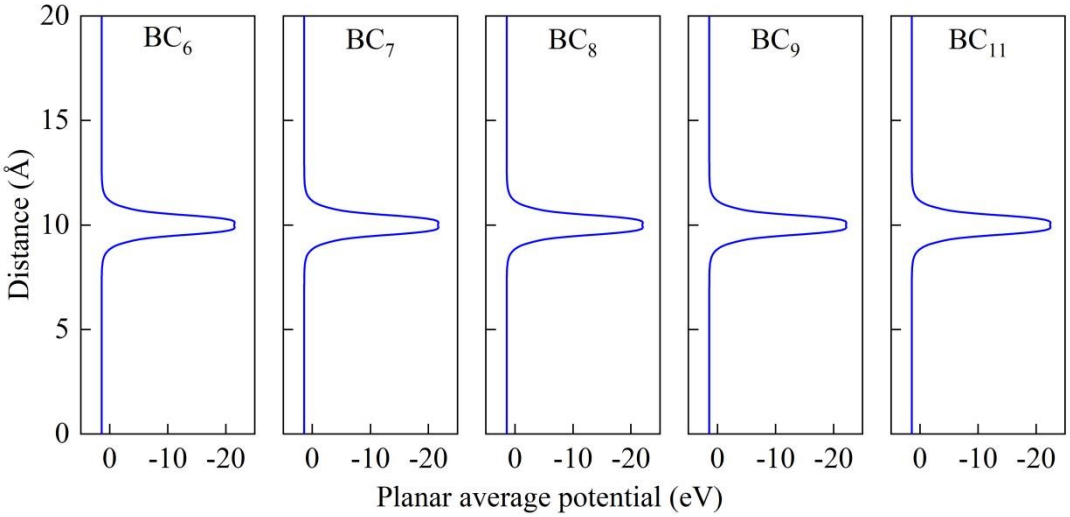

Fig. S1 The planar average potential as a function of the distance along the *c*-axis for five B–C monolayers. Only the B–C layer (located at 10 Å) exhibits an obvious planar average potential, while the vacuum layer is flat, which indicates that there is no interlayer interaction between adjacent layers.

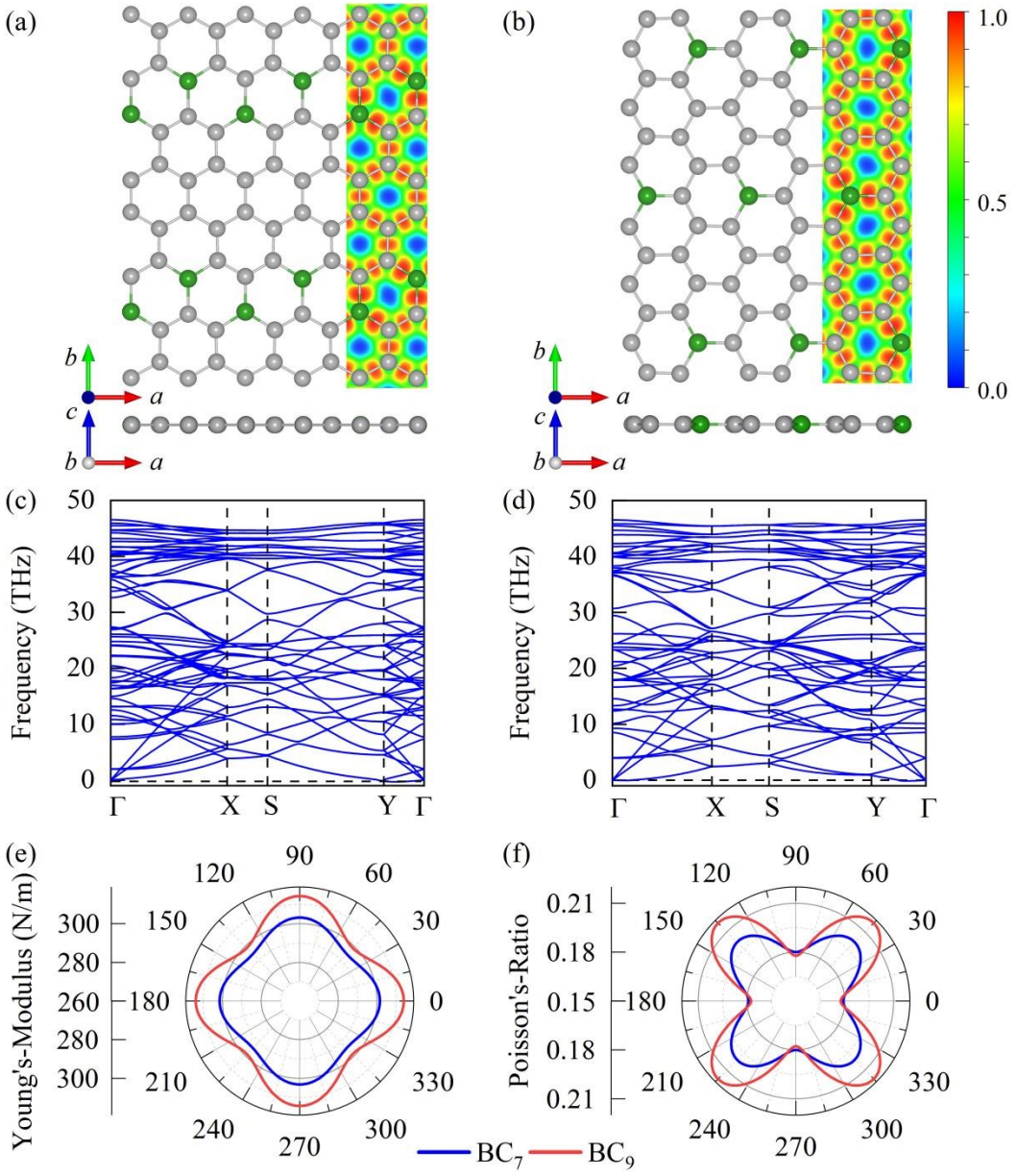

Fig. S2 (a)-(b) Crystal structures and (c)-(d) phonon spectra of BC_7 and BC_9 monolayers, respectively. The structures also include the electron local function (ELF). (e) represents their Young's modulus, and (f) represents their Poisson's ratio.

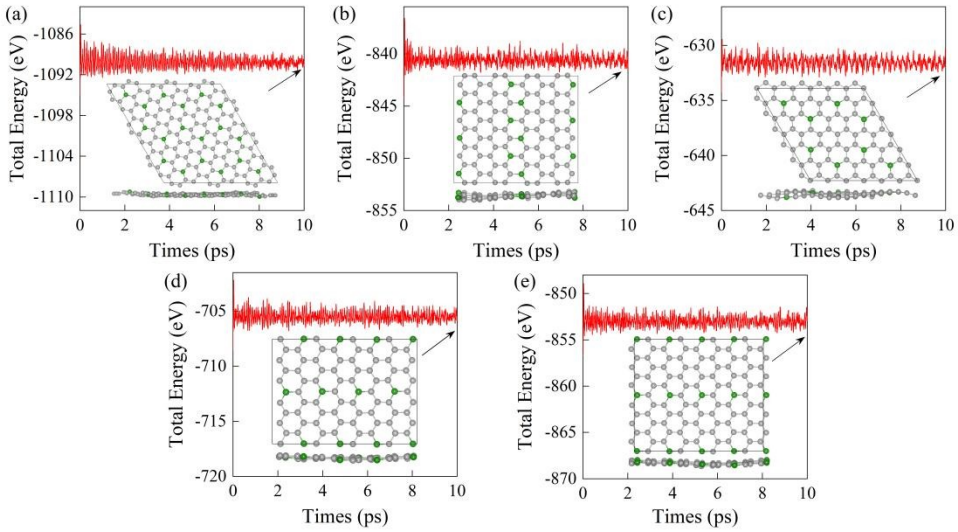

Fig. S3 AIMD simulations for (a) BC_6, (b) BC_7, (c) BC_8, (d) BC_9, and (e) BC_{11} monolayers at 300 K. The inset gives top and side view of the structure after 10 ps.

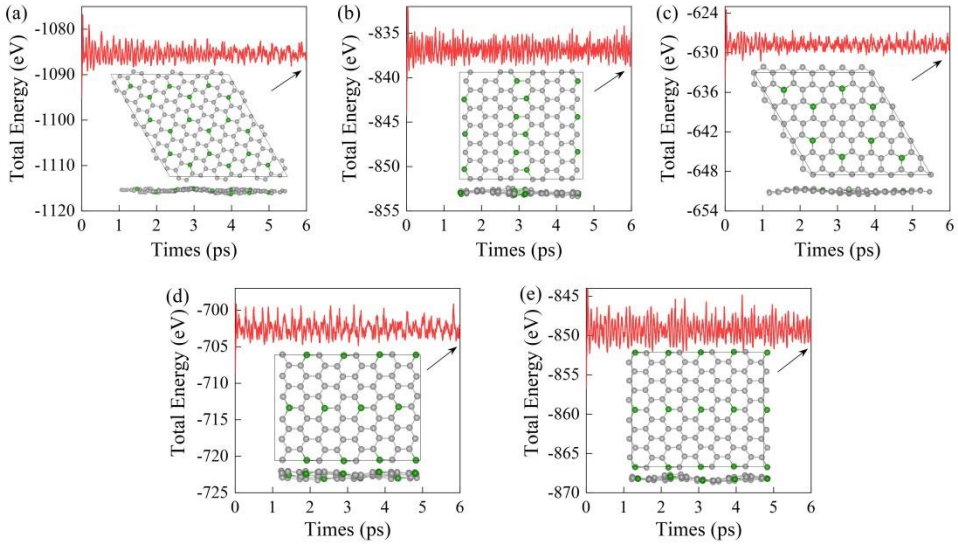

Fig. S4 AIMD simulations for (a) BC_6, (b) BC_7, (c) BC_8, (d) BC_9, and (e) BC_{11} monolayers at 600 K. The inset gives top and side view of the structure after 6 ps. Total energy remains equilibrium and the structures are not fractured or collapsed, indicating that they are thermal stable.

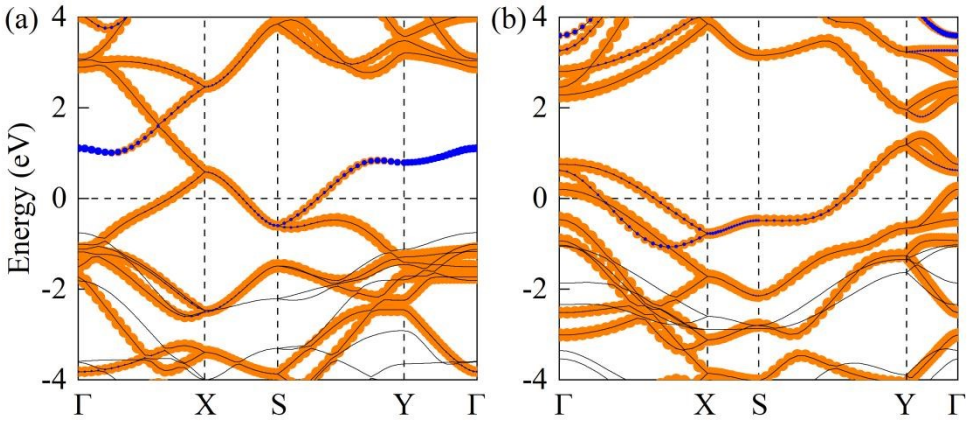

Fig. S5 Projected band structures of (a) BC_7 and (b) BC_9 monolayers. The metallic property is mainly contributed by the p_z orbitals, hence here only the p_z orbitals of C (yellow) and B (blue) are given.

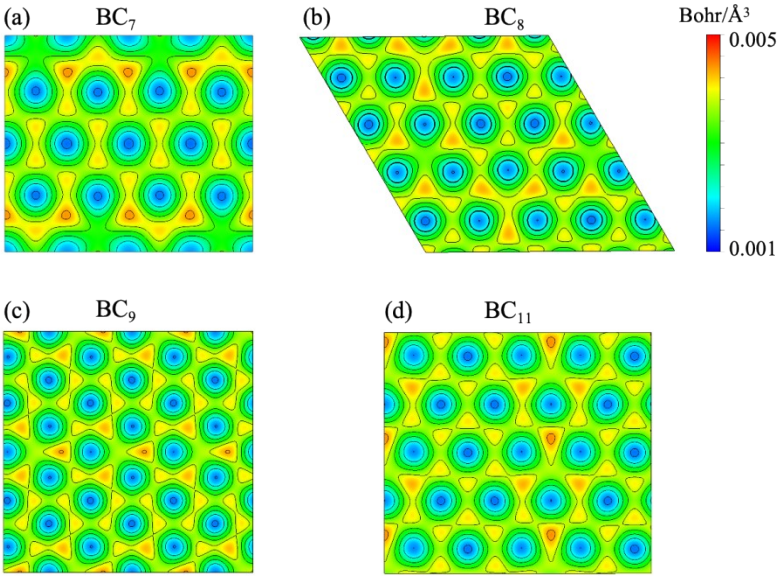

Fig. S6 Charge density in the plane 1.6 Å above the sheet for (a) BC_7, (b) BC_8, (c) BC_9, and (d) BC_{11}, respectively.

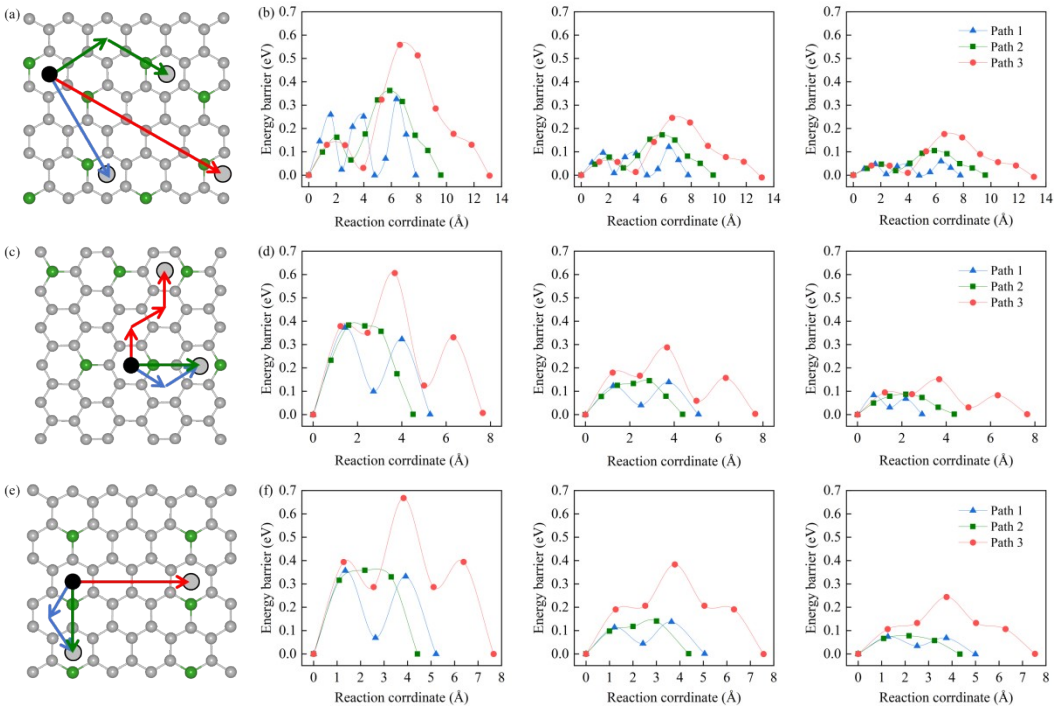

Fig. S7 Ion migration paths on the (a) BC_8 and (c) BC_9 and (e) BC_{11} monolayers. Green, red, and blue indicate different paths. The corresponding CI-NEB migration barriers of Li, Na, and K across three paths are depicted in (b), (d), and (f). The blue path has the lowest barrier, with Li, Na, and K ion migration energy barriers of 0.33, 0.12, and 0.06 eV for BC_8, 0.37, 0.14, and 0.08 eV for BC_9 and 0.36, 0.14, and 0.07 eV for BC_{11}, respectively.

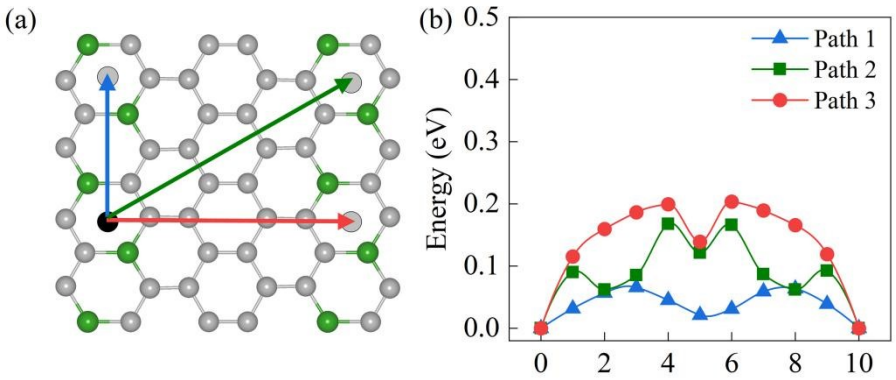

Fig. S8 (a) The migration pathways of K ions and (b) their corresponding CI-NEB migration barriers for the three pathways in BC_7. The Path 1 (in blue) represents the minimum K-ion migration path with migration energy barrier of 0.07 eV. It is noted that the BC_7 most stable adsorption site is on the center of B_2C_4 ring, and the optimal migration path is also along the center of B_2C_4 rings.

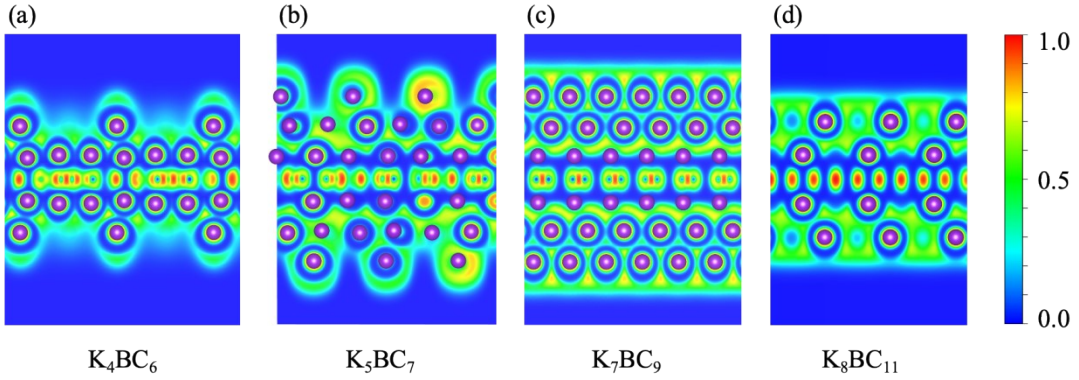

Fig. S9 ELF snapshots of K loaded on (a) K_4BC_6, (b) K_5BC_7, (c) K_7BC_9, and (d) K_8BC_{11}, respectively. There is significant localization of the electrons between the K ions, which act as anionic electrons to minimize the repulsion between the K ions, thereby increasing the theoretical capacity.

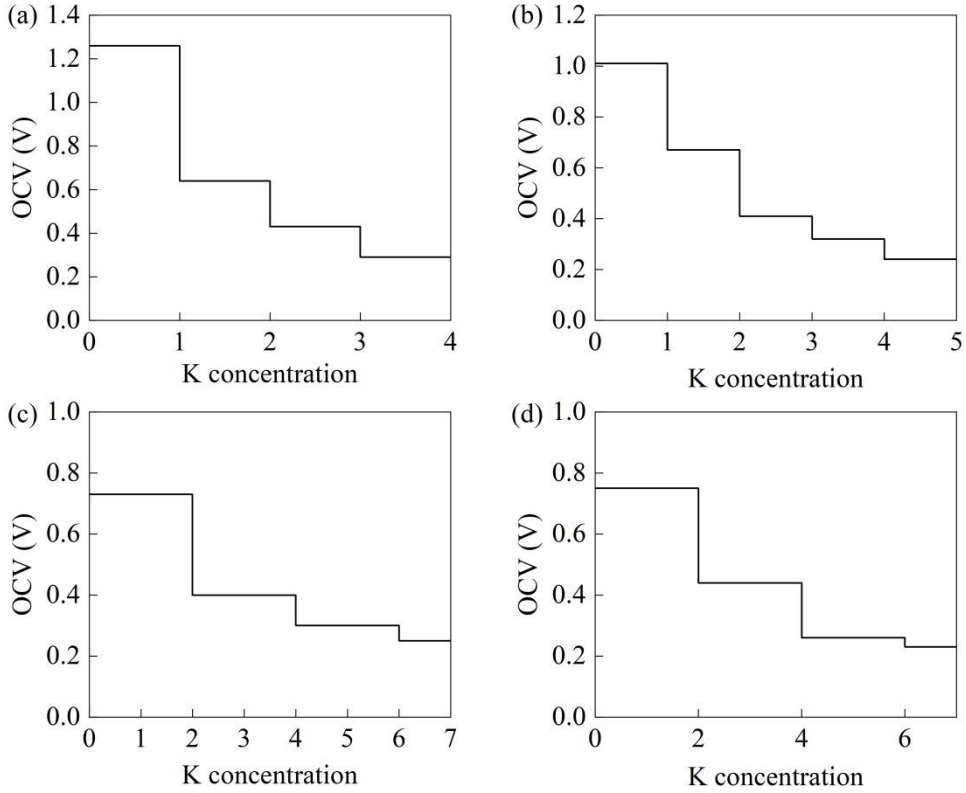

Fig. S10 OCV as a function of K concentration in (a) BC_6, (b) BC_7, (c) BC_9, and (d) BC_{11}, respectively.

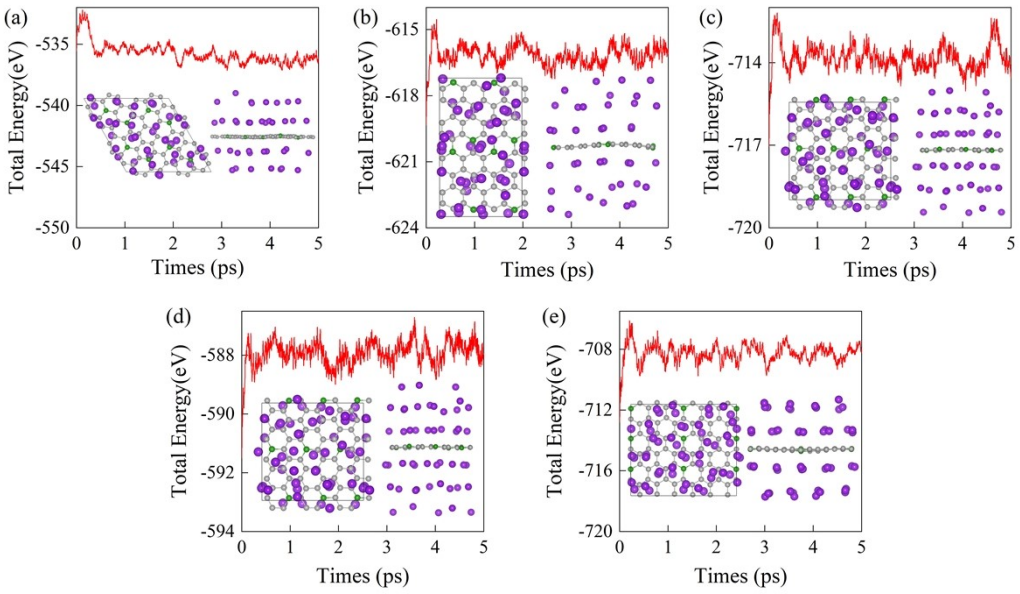

Fig. S11 AIMD simulations of K_4BC_6, K_5BC_7, K_7BC_8, K_7BC_9, and K_8BC_{11} at 300 K. The inset gives top and side view of the structure after 5 ps.

Supplementary Tables

Table S1 Structural information of the five B–C monolayers.

	Space group	Lattice Parameters	Wyckoff Positions (fractional)			
			Atoms	*x*	*y*	*z*
BC_6	*P*6/*m*	*a* = *b* = 6.6889 Å	B (2 *d*)	0.33333	0.66667	0.50000
		c = 20.0000 Å	C_1 (6 *k*)	0.76909	0.80564	0.50000
			C_2 (6 *k*)	0.91432	0.53130	0.50000
BC_7	*Pmma*	*a* = 5.0404 Å	B (2 *f*)	0.75000	0.50000	-0.08341
		b = 20.0000 Å	C_1 (2 *f*)	0.75000	0.50000	-0.90458
		c = 8.7524 Å	C_2 (2 *f*)	0.75000	0.50000	-0.41753
			C_3 (2 *f*)	0.75000	0.50000	-0.57941
			C_4 (4 *j*)	0.50746	0.50000	-0.82478
			C_5 (4 *j*)	0.00200	0.50000	-0.33739
BC_8	*P*-6*m*2	*a* = *b* = 7.5423 Å	B_1 (1 *f*)	0.66667	0.33333	0.50000
		c = 20.0000 Å	B_2 (1 *d*)	0.33333	0.66667	0.50000
			C_1 (6 *m*)	0.66785	0.99859	0.50000
			C_2 (3 *k*)	0.56470	0.78235	0.50000
			C_3 (1 *b*)	0.00000	0.00000	0.50000
			C_4 (3 *k*)	0.22208	0.11104	0.50000
			C_5 (3 *k*)	0.89720	0.44860	0.50000
BC_9	*Amm*2	*a* = 20.0000 Å	B (2 *b*)	0.50000	0.00000	-0.88377
		b = 12.5524 Å	C_1 (2 *b*)	0.50000	0.00000	-0.23045
		c = 4.3433 Å	C_2 (4 *e*)	0.50000	0.29739	-0.37703
			C_3 (4 *e*)	0.50000	0.39874	-0.88453
			C_4 (4 *e*)	0.50000	0.19966	-0.21179
			C_5 (4 *e*)	0.50000	0.39490	-0.21027
BC_{11}	*Pmm*2	*a* = 7.5152 Å	B (1 *b*)	0.00000	0.50000	-0.90610

b = 20.0000 Å	C_1 (1 b)	0.00000	0.50000	-0.56093
c = 4.3269 Å	C_2 (2 f)	0.83037	0.50000	-0.40628
	C_3 (2 f)	0.33507	0.50000	-0.57926
	C_4 (2 f)	0.82515	0.50000	-0.07969
	C_5 (2 f)	0.66310	0.50000	-0.91249
	C_6 (1 d)	0.50000	0.50000	-0.41294
	C_7 (1 d)	0.50000	0.50000	-0.07828

Table S2 Comparison of five B–C monolayers with reported 2D materials for cohesion energy (E_{coh}).

	E_{coh} (eV/atom)	Ref.
Silicene	–3.71	[8, 9]
Phosphorene	–3.61	[10, 11]
C_5N_2	–6.74 ~ –6.78	[12]
BC_3	–8.33	[13]
B_4C_3	–6.89	[14]
B_3C_2	–6.83 ~ –6.87	
B_2C	–6.75	
B_4C	–6.46	
BC_7	–8.66	[15-17]
B_5C_8	–7.68	[4]
BC_6	–8.61	This study
BC_7	–8.72	This study
BC_8	–8.73	This study
BC_9	–8.78	This study
BC_{11}	–8.84	This study

Table S3 The elastic constants (C_{ij} in N/m), average Young's modulus (E in N/m), and average Poisson's ratios (v) of the five B–C monolayers. The values of C_{ij} satisfy the Born criteria, indicating mechanical stability.

	C_{11}	C_{12}	C_{22}	C_{66}	E	v
BC_6	300.27	65.89	300.27	117.20	285.82	0.22
BC_7	311.50	56.08	313.22	122.55	298.31	0.19
BC_8	315.29	62.78	315.29	126.26	302.79	0.20
BC_9	324.05	57.60	324.47	122.69	306.31	0.20
BC_{11}	325.05	62.92	325.78	131.57	313.48	0.19

Table S4 The variation of lattice constants (*a*, *b* in Å) for the five K adsorbed B–C monolayers as a function of K concentration.

Material	K concentration	*a*	*b*	% change in *a*	% change in *b*	Average change in the *ab* plane
BC_6	K_0BC_6	6.689	6.689			
	K_1BC_6	6.713	6.725	0.359	0.538	0.449
	K_2BC_6	6.726	6.730	0.553	0.613	0.583
	K_3BC_6	6.763	6.766	1.106	1.151	1.129
	K_4BC_6	6.758	6.762	1.032	1.091	1.062
BC_7	K_0BC_7	5.040	8.752			
	K_1BC_7	5.061	8.783	0.417	0.354	0.386
	K_2BC_7	5.058	8.773	0.357	0.240	0.299
	K_3BC_7	5.058	8.775	0.357	0.263	0.310
	K_4BC_7	5.050	8.783	0.198	0.354	0.276
	K_5BC_7	5.048	8.762	0.159	0.114	0.137
BC_8	K_0BC_8	7.542	7.542			
	K_1BC_8	7.576	7.576	0.451	0.451	0.451
	K_2BC_8	7.577	7.578	0.464	0.477	0.471
	K_3BC_8	7.588	7.588	0.610	0.610	0.610
	K_4BC_8	7.593	7.594	0.676	0.689	0.683
	K_5BC_8	7.594	7.595	0.689	0.703	0.696
	K_6BC_8	7.604	7.604	0.822	0.822	0.822
	K_7BC_8	7.608	7.609	0.875	0.888	0.882
BC_9	K_0BC_9	4.343	12.552			
	K_2BC_9	4.365	12.583	0.507	0.247	0.377
	K_4BC_9	4.367	12.610	0.553	0.462	0.508
	K_6BC_9	4.374	12.601	0.714	0.390	0.552
	K_7BC_9	4.378	12.600	0.806	0.382	0.594
BC_{11}	K_0BC_{11}	7.515	4.327			
	K_2BC_{11}	7.530	4.352	0.200	0.578	0.389
	K_4BC_{11}	7.555	4.360	0.532	0.763	0.648
	K_6BC_{11}	7.549	4.364	0.452	0.855	0.654
	K_8BC_{11}	7.571	4.370	0.745	0.994	0.870

Table S5 The elastic constants (C_{ij} in N/m), average Young's modulus (E in N/m), and average Poisson's ratios (v) of the five fully potassiated B–C monolayers. The values of C_{ij} satisfy the Born criteria, indicating mechanical stability.

	C_{11}	C_{12}	C_{22}	C_{66}	E	v
BC_6	280.83	58.12	280.83	111.35	268.80	0.21
BC_7	309.39	56.69	311.14	121.98	296.48	0.19
BC_8	297.61	57.60	297.61	120.00	286.46	0.19
BC_9	310.71	54.92	314.41	118.83	295.70	0.20
BC_{11}	308.65	57.13	307.95	126.20	298.15	0.18

References

1. Y. Wang, J. Lv, L. Zhu and Y. Ma, *Phys. Rev. B*, 2010, **82**, 094116.
2. Y. Wang, J. Lv, L. Zhu and Y. Ma, *Computer. Phys. Commun.*, 2012, **183**, 2063-2070.
3. X. Yu, X. Chen, X. Wang, Z. Yuan, J. Feng and J. Rong, *Chem. Eng. J.*, 2021, **406**, 126812.
4. H.-B. Cao, X.-H. Wang, X. Xiong, C.-S. Liu and X.-J. Ye, *Appl. Phys. Lett.*, 2024, **124**, 073908.
5. G. Kresse and J. Furthmüller, *Phys. Rev. B*, 1996, **54**, 11169.
6. J. P. Perdew, K. Burke and M. Ernzerhof, *Phys. Rev. Lett.*, 1996, **77**, 3865-3868.
7. https://github.com/tamaswells/VASP_script/blob/master/scan_adsorption_energy.py.
8. B. Feng, Z. Ding, S. Meng, Y. Yao, X. He, P. Cheng, L. Chen and K. Wu, *Nano. Lett.*, 2012, **12**, 3507-3511.
9. A. Fleurence, R. Friedlein, T. Ozaki, H. Kawai, Y. Wang and Y. Yamada-Takamura, *Phys. Rev. Lett.*, 2012, **108**, 245501.
10. H. Liu, A. T. Neal, Z. Zhu, Z. Luo, X. Xu, D. Tománek and P. D. Ye, *ACS Nano*, 2014, **8**, 4033-4041.
11. D. Li, M. Chen, Z. Sun, P. Yu, Z. Liu, P. M. Ajayan and Z. Zhang, *Nat. Nanotechnol.*, 2017, **12**, 901-906.
12. M. You, G. Guo, Y. Liao, S. Luo, C. He, C. Tang and J. Zhong, *J. Energy Storage*, 2024, **84**, 111004.
13. H. Zhang, Y. Liao, G. Yang and X. Zhou, *ACS Omega*, 2018, **3**, 10517-10525.
14. D. Fan, S. Lu, Y. Guo and X. Hu, *J. Mater. Chem. C*, 2018, **6**, 1651-1658.
15. D. Das, R. P. Hardikar, S. S. Han, K. R. Lee and A. K. Singh, *Phys. Chem. Chem. Phys.*, 2017, **19**, 24230-24239.
16. S. Gong and Q. Wang, *J. Phys. Chem. C*, 2017, **121**, 24418-24424.
17. A. P. Durajski and G. T. Kasprzak, *Physica B*, 2023, **660**, 414902.